Optics and Lasers in Engineering 62 (2014) 9–16

Contents lists available at ScienceDirect

Optics and Lasers in Engineering

journal homepage: www.elsevier.com/locate/optlaseng

Nanosecond laser texturing for high friction applications

Andrew Dunn [a,*], Jesper V. Carstensen [b], Krystian L. Wlodarczyk [a], Erica B. Hansen [b], Jack Gabzdyl [c], Paul M. Harrison [c], Jonathan D. Shephard [a], Duncan P. Hand [a]

[a] Institute of Photonics and Quantum Sciences, Heriot-Watt University, Edinburgh, Scotland EH14 4AS, UK
[b] MAN Diesel & Turbo, Teglholmsgade 41, 2450 Copenhagen SV, Denmark
[c] SPI Lasers UK Ltd., Wellington Park, Tollbar Way, Hedge End, Southampton SO30 2QU, UK

ARTICLE INFO

Article history:
Received 5 February 2014
Received in revised form
17 April 2014
Accepted 11 May 2014
Available online 29 May 2014

Keywords:
Laser texturing
Surface processing
High friction
Fibre laser

ABSTRACT

A nanosecond pulsed Nd:YAG fibre laser with wavelength of 1064 nm was used to texture several different steels, including grade 304 stainless steel, grade 316 stainless steel, Cr–Mo–Al 'nitriding' steel and low alloy carbon steel, in order to generate surfaces with a high static friction coefficient. Such surfaces have applications, for example, in large engines to reduce the tightening forces required for a joint or to secure precision fittings easily. For the generation of high friction textures, a hexagonal arrangement of laser pulses was used with various pulse overlaps and pulse energies. Friction testing of the samples suggests that the pulse energy should be high (around 0.8 mJ) and the laser pulse overlap should be higher than 50% in order to achieve a static friction coefficient of more than 0.5. It was also noted that laser processing increases the surface hardness of samples which appears to correlate with the increase in friction. Energy-Dispersive X-ray spectroscopy (EDX) measurements indicate that this hardness is caused by the formation of hard metal-oxides at the material surface.

1. Introduction

Surface engineering is a common application for high power lasers and a significant amount of research is currently taking place in this field. This is partly driven by the benefits, particularly for industrial applications, that can be gained from improvements in the surface properties of engineering materials. Lasers have many properties which are advantageous for use in surface engineering such as their flexibility, accuracy, speed, lack of tool wear as well as the negligible effect the processes have on the properties of the bulk material [1,2]. There are other methods which have been used to modify surface properties, such as electron beam treatment [3,4], chemical treatment [5], plasma treatment [6], electric discharge [7] and sand blasting [8], each of which are used for a variety of applications within surface engineering.

One of the most studied applications for laser surface texturing is the reduction of friction, both static and kinetic. This application is primarily based on the generation of indentations in the material surface which can then be filled with lubricant. The indentations therefore act as micro-hydrodynamic bearings [9], lubricant reservoirs or as traps for wear debris [2,10], depending on the lubrication regime. These indentations can take various forms. Most commonly, simple 'dimples' are generated in an array by ablation at discrete locations, with dimensions varying from 50–300 μm diameter with 5–80 μm depth [11,12]. Other feature geometries may also be used such as micro-grooves, which can be manufactured by the ablation of a series of parallel lines [13]. Another approach is the generation of a 'cross-like' structure using laser interference metallurgy [14]. The key parameters for generating a low friction surface appear to be the dimple density, diameter and depth [13,15,16]. In most cases, a dimple density in the region of 5–10% appears to be most effective at reducing the friction coefficient [13,16], however dimple dimensions are more dependent on the contact regime [15]. As a result, with the selection of the correct parameters for the desired application, laser surface texturing can lower the coefficient of friction by 20% or more [13,14].

Despite all the current research in the field of laser texturing for friction applications, very little appears to have been reported with regards to actively increasing the friction coefficient of a surface. It has been shown that laser surface texturing can increase the friction between two components under certain conditions [15,17]; however, at present, this has only been reported for sliding friction tests where increased friction is undesirable due to the resulting increase in wear. Applications for high static friction surfaces include the reduction of the tightening forces required for a joint or to secure a precision fitting easily [18]. These applications are particularly relevant where the components in question are very large and so are expensive and/or difficult to machine with the required precision.

* Corresponding author. Tel.: +44 1314513086.
E-mail address: ad134@hw.ac.uk (A. Dunn).

http://dx.doi.org/10.1016/j.optlaseng.2014.05.003

This paper describes the characterisation of laser generated surface features followed by initial design and testing of laser generated, high friction surfaces. Applications for such high friction surfaces include friction discs [18]. MAN Diesel & Turbo (MDT), for example, are looking for a reliable method of generating high static friction surfaces ($\mu_s > 0.6$) for use in components of large engines. The work detailed in this paper aimed to achieve static friction coefficients of more than 0.6 for applied normal forces in the range 20-60 kN, as required for this application. Unlike the textures generated for friction reduction, where arrays of discrete dimples are normally used, here pulses were overlapped to generate rougher surfaces.

2. Experimental

2.1. Experimental set-up

Prior to performing friction tests, the size and shape of laser induced craters and troughs were characterised for various processing settings, in particular pulse energy and number of pulses. For this characterisation, a pulsed SPI 20WL laser ($M^2 \sim 1.8$) was used with wavelength of 1064 nm, pulse duration of ~200 ns, maximum pulse energy of 0.8 mJ and nominal spot size of ~50 μm ($1/e^2$ of maximum intensity). The low cost, high flexibility and acceptable absorption of this wavelength make this type of laser well suited for surface texturing. The craters were made by 1–5 pulses repeated in the same location whilst the troughs were created by generating a line of overlapping pulses using a pulse repetition rate of 25 kHz and varying the laser scan speed. The laser beam was scanned using a galvanometric scanner with an F-theta focussing lens and controlled by a PC using SCAPS Samlight software. Initial characterisation tests were performed on commercially available, grade 304 stainless steel (SS304) with further tests performed on Cr–Mo–Al 'nitriding' steel in order to confirm the observed trends. The laser processing set-up used is shown in Fig. 1.

2.2. Characterisation and texturing

A matrix of individual craters was generated on the SS304 by varying the pulse energy between 0.16 mJ and 0.8 mJ and varying the number of pulses for each crater between 1 and 5. The depth and diameter of these craters were then measured with an optical microscope (Leica DM6000M) with depth measurement capability.

By varying the laser scan speed between 62.5 mm/s and 1250 mm/s, lines were generated for a range of laser pulse overlaps (from 0% to 95%). This was performed on the nitriding steel at two selected pulse energies, 0.4 mJ and 0.8 mJ, with the width and depth of the resulting troughs measured optically.

A two dimensional 'hexagonal' arrangement of pulses was used, as shown in Fig. 2, in order to generate a homogeneous surface structure with the aim of achieving a consistent friction coefficient, regardless of the direction of motion. Three different materials were used for friction testing; Cr–Mo–Al 'nitriding' steel, stainless steel grade 316 (SS316) and low alloy carbon steel.

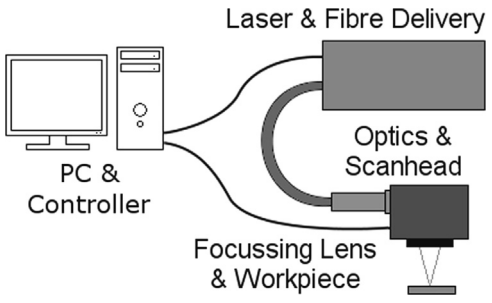

Fig. 1. Schematic of laser processing workstation with the fibre laser and galvo scanner controlled by the PC software and controller.

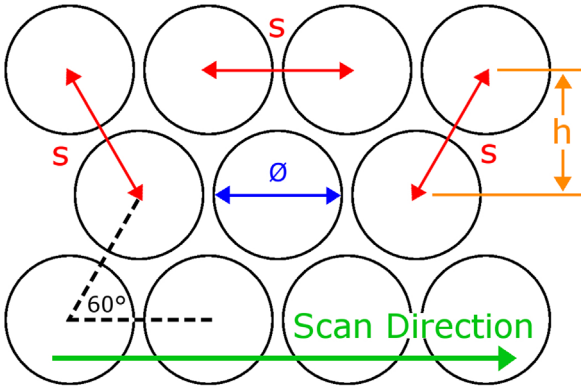

Fig. 2. Schematic of 'hexagonal' laser pulse layout used for high friction texturing where d is pulse diameter, s is the pulse separation and h is the hatch distance.

The design of this pulse layout was maintained throughout; however the laser pulse overlap was used as a variable. This was achieved by modifying the scan speed and hatch distance, h. The pulse overlap was calculated as follows:

$$\text{Overlap} = \frac{\varnothing - (\text{Rep. Rate} \times v)}{\varnothing} \times 100\% \quad (1)$$

where $\varnothing$ is the pulse width (laser beam diameter), v is the scan speed and Rep. Rate is the pulse repetition rate. In order to maintain the hexagonal shape of the pulse layout, the hatch distance must also be altered accordingly:

$$h = \cos(30^\circ) \times (\text{Rep. Rate} \times v). \quad (2)$$

2.3. Measurement and testing

As mentioned in Section 2.2, an optical microscope was used to obtain both images and depth data for the processed samples. This data also allowed surface roughness parameters to be calculated prior to the friction testing. In order to test the friction coefficient of the textured samples, both (opposite) faces of the samples were processed and then placed in the friction testing set-up, as shown in Fig. 3a.

The sample to be tested is placed between two standard counter surface pieces (untextured, made of low alloy steel ground to $R_a = 0.4$ μm) which are held within two larger steel blocks, as seen in Fig. 3b. The counter surfaces in the testing set-up are untextured due to the MDT application, where texturing of the complete engine component is unfeasible and so only a thin shim is to be textured and placed between the components. The cavities in which the counter surface pieces are held are shallow, such that the counter surfaces protrude from the surfaces of the steel blocks, thus allowing the sample to be in contact only with the two counter surfaces. Normal force is applied to the sample, through the counter surface pieces and steel blocks (and load cell), by two high strength steel bolts. For the MDT application, the normal force is required to be between 20 kN and 60 kN; providing a pressure of 50–150 MPa on the surfaces of the sample. A miniature load cell (strain gauge) is used to measure the force which is applied to the sample directly. This set-up can be seen in Fig. 3, with the sample in place and ready to test with a hydraulic press (100 kN Dartec).

Once the normal force has been applied to the sample by tightening the two bolts appropriately, the test set-up is moved to

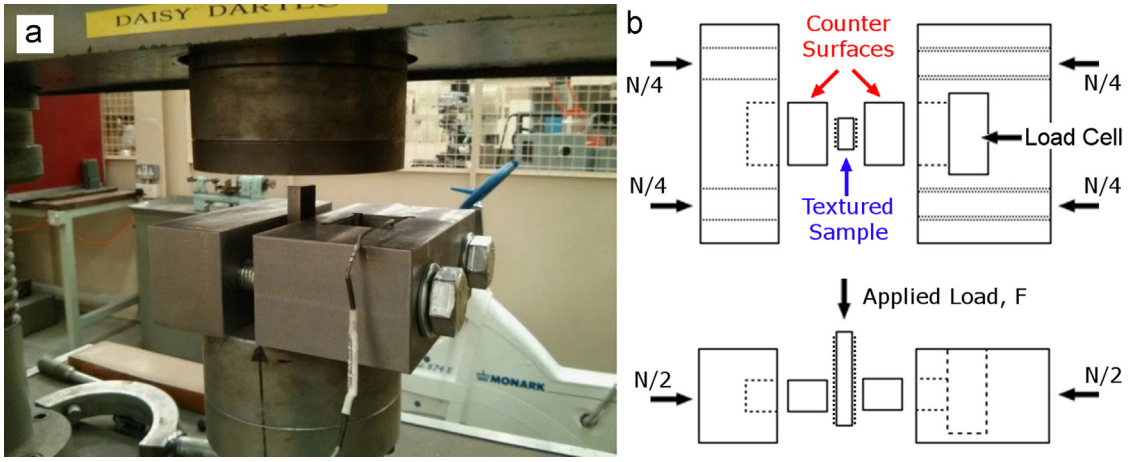

Fig. 3. Friction testing set-up on the Dartec hydraulic press with sample held by the normal force, which is applied by the two bolts (a) and schematic of testing rig showing sample, counter surfaces and applied forces (*N* denotes normal force) from top-down view (top) and side-on (bottom) views (b).

the hydraulic press. This is used to apply the load force (which is recorded on a PC along with the 'stroke' distance) to the sample which is gradually increased until the sample slips. The force applied at the point of slipping denotes the maximum load force, F_{max}, which is used to calculate the coefficient of static friction, as follows:

$$\mu_s = \frac{F_{max}}{2N} \tag{3}$$

where N is the normal force applied to the sample by the bolts. The factor of two relates to the fact that both surfaces of the sample are under test. Upon slipping, the sample was deemed to have 'failed', as a real component would require replacement at this point for the MDT application, and so testing of the samples was stopped at this point.

Hardness testing was performed on the laser textured surfaces using a diamond tipped Vickers hardness macro-indenter using a load of 30 kg f for ~10 s. The resulting indents were then measured optically with the Vickers hardness calculated as follows:

$$H_v = \frac{2F \sin(136^\circ/2)}{d^2}. \tag{4}$$

3. Results and discussion

3.1. Characterisation of individual craters

3.1.1. Impact of laser pulses

The effect of increasing number of pulses was studied. The number of pulses per crater was varied between one and five for each array of craters generated at various pulse energies. Crater depth was found to increase linearly with number of pulses for pulse energies greater than the ablation threshold (~0.2 mJ, ~10 J cm^{-2}), as shown in Fig. 4.

The results show an approximately linear trend which confirms that each pulse (with energy above the ablation threshold) removes approximately the same depth of material from the crater. Given that the temporal pulse spacing is sufficient to allow the sample to reach thermal equilibrium between consecutive pulses and the change in depth being significantly less than the Rayleigh range (~1.8 mm) of the focussed laser beam, this was the expected result. The diameters of the craters were then measured. Fig. 5 shows that the diameter of the crater is independent of the number of pulses used. Since the laser pulses are repeated at the same point on the sample, the area of the crater where the laser fluence is above the ablation threshold remains constant and so the diameter of the crater remains constant, regardless of the number of pulses.

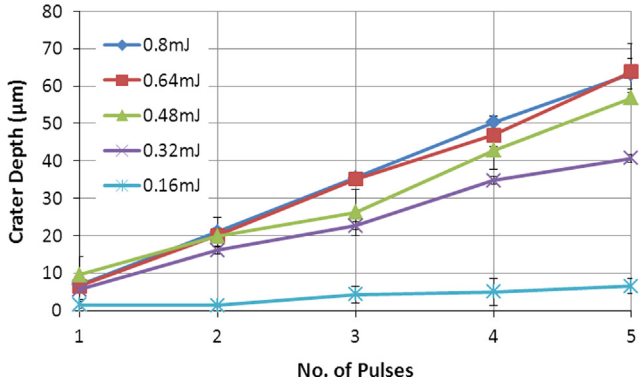

Fig. 4. Crater depth as a function of number of pulses for different pulse energies.

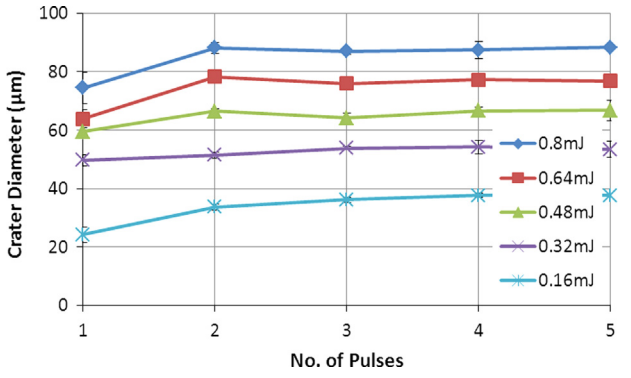

Fig. 5. Crater diameter as a function of number of pulses for different pulse energies.

3.1.2. Impact of pulse energy

By replotting the data from Section 3.1.1, the dependence of the crater depth and diameter on the pulse energy can be observed, as shown in Fig. 6.

In contrast to the results where the number of pulses was varied, the crater depth was found to be almost unchanged by changes in pulse energy when above the ablation threshold, whilst the diameter increased linearly with pulse energy. The crater

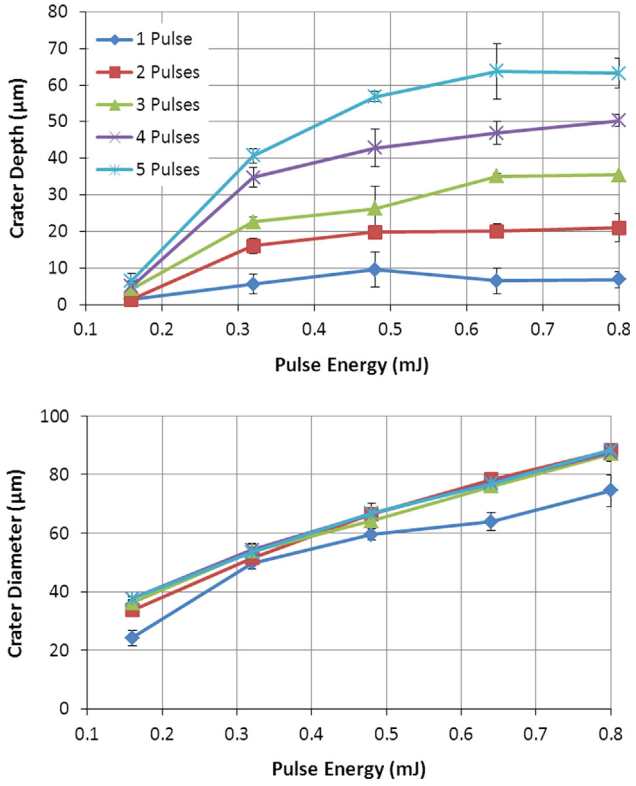

Fig. 6. Crater depth (top) and diameter (bottom) as a function of pulse energy for different number of pulses.

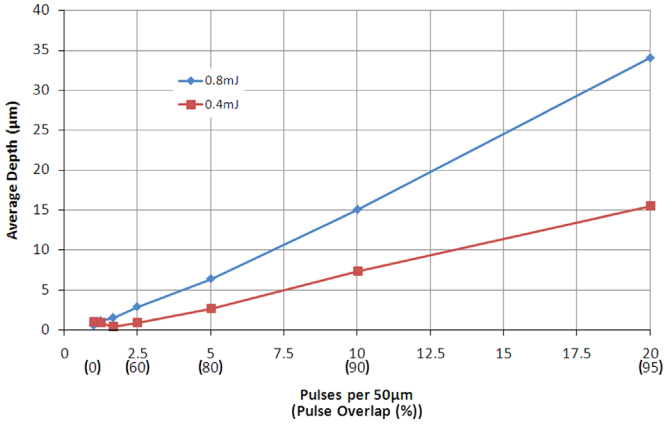

Fig. 7. Average trough depth as function of spatial pulse density.

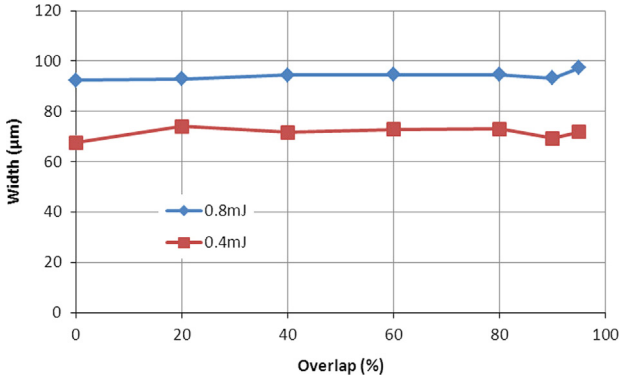

Fig. 8. Trough width as a function of pulse overlap.

diameter, however, is very much dependent on the area of the central part of the beam for which the fluence exceeds the ablation threshold, explaining the dependence on pulse energy. The results shown in Figs. 4–6 are the averages of 3 separate measurements obtained from the optical microscope mentioned in Section 2.2. The error bars plotted on these graphs are the standard deviations of three measurements for each point and, as can be seen from the figures, is typically «5 µm, indicating that the features formed by the laser pulses are very uniform. This agrees with what was seen by visually inspecting the sample after laser processing.

From these results, which are largely in agreement with those obtained by Vilhena et al. [15] for both pulse energy and number of pulses, it is clear that it is possible to independently control both crater depth and diameter. Thus, by using the correct number of pulses and pulse energy used to generate the crater, the crater dimensions that are required can be easily obtained.

3.2. Overlapping pulses

Prior to generating area textures, the effect of overlapping pulses was studied on nitriding steel. By using a laser repetition rate of 25 kHz and varying the beam scan speed between 62.5 mm/s and 1250 mm/s, pulse overlaps in the range of 0–95% were achieved and used to machine single lines.

Fig. 7 shows that the depth of the trough generated increased linearly with the number of pulses per distance; here 50 µm was chosen as this corresponds to the nominal spot diameter. This is in agreement with the individual crater results which showed a linear increase with number of pulses. The observed difference between the two pulse energies is likely due to the difference in area which is ablated with each pulse; clearly the area for 0.4 mJ pulses is smaller. As a result, the effective pulse overlap is decreased and so the depth per pulse achieved is significantly lower. The widths of the troughs were also measured, as shown in Fig. 8.

The widths of the troughs were found to be independent from the pulse overlap, in agreement with the independence of the crater diameter from the number of pulses. The trough generated with pulses of 0.8 mJ was also found to be wider than the 0.4 mJ trough, as predicted from the individual crater results.

3.3. Friction and hardness

3.3.1. Pulse overlap and pulse energy

Following the results obtained in Sections 3.1 and 3.2, the effect of varying pulse energy and pulse overlap on the friction coefficient was examined. Pulse energies of 0.4 mJ and 0.8 mJ were chosen for the initial study as these are both above the ablation threshold ($\sim$0.2 mJ, $\sim$10 J cm^{-2}), determined from the individual crater analysis, whilst generating very different surface structures. For the 0.4 mJ pulses, the surface features were dominated by melt effects, as shown in Fig. 9a, whereas for 0.8 mJ pulses the ablation was much more apparent (shown in Fig. 9b). As a result, the higher energy pulse texture gives a fine, rough surface whilst the texture obtained from the low energy pulses give a smoother surface. Pulse overlap was varied between $-$50% and 85% in the hexagonal arrangement outlined in Section 2.2 in order to achieve a range of surface roughness values. From the results shown in Section 3.2, higher pulse overlap was expected to give larger peak-to-trough heights and result in higher surface roughness' and friction coefficients.

The initial friction tests were performed using the set-up described in Section 2.3 with a normal force of 60 kN (150 MPa). These tests were carried out on nitriding steel samples with the results shown in Fig. 10.

When the textures are generated by 0.4 mJ pulses, there is a general trend of the friction coefficient increasing with pulse

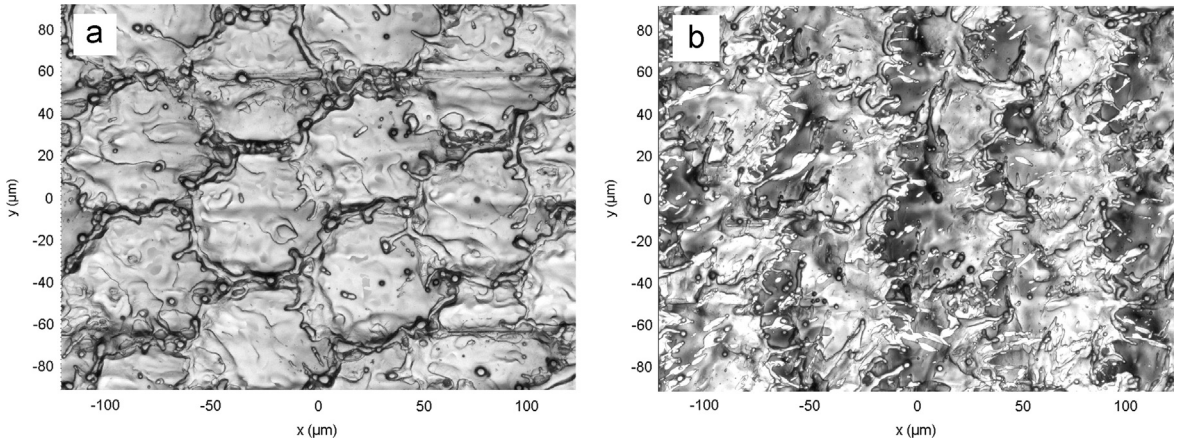

Fig. 9. Micrograph of 0.4 mJ (a) and 0.8 mJ (b) pulse textures at −25% pulse overlap showing melt and ablation features, respectively.

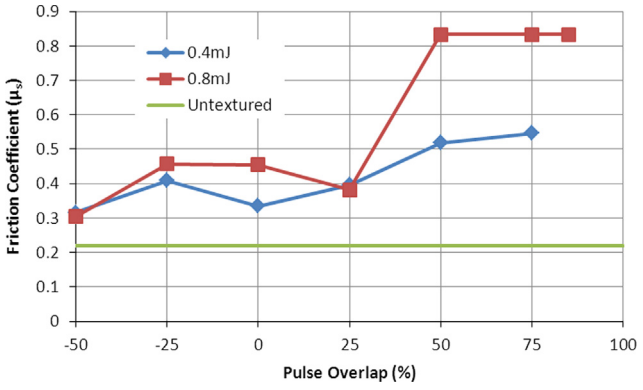

Fig. 10. Dependence of friction coefficient on pulse overlap for low (0.4 mJ) and high (0.8 mJ) pulse energies with the result obtained from untextured samples given as a baseline (normal=60 kN).

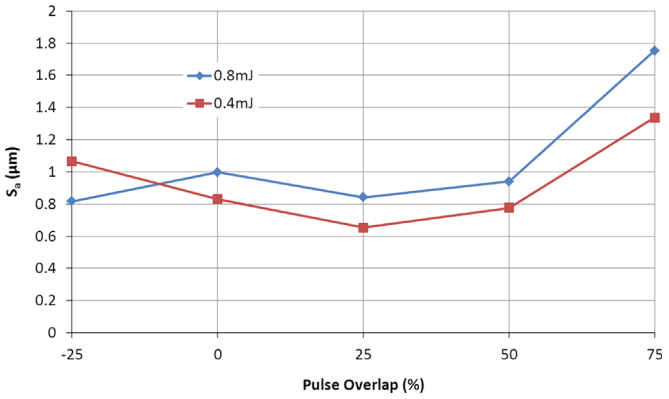

Fig. 11. Arithmetic average surface roughness, S_a, as a function of pulse overlap.

overlap with a maximum of $\mu_s=0.55$ for 75% pulse overlap. For the higher pulse energy, this trend is also visible (with the exception of ~25% pulse overlap), with a greater increase in friction observed at high pulse overlaps (>50%). For these textures, the load force required to cause the sample to slip exceeded the 100 kN force available from the hydraulic press and, as a result, the friction coefficient in this region is at least 0.83, however it was not possible to determine the exact value. Following these results, the normal force applied in later tests was reduced to 40 kN (100 MPa). It is clear from the results that using higher pulse energies consistently gives higher friction coefficients for the same value of pulse overlap. Also, a value of $\mu_s=0.22$ was obtained for the as-received nitriding steel under the same testing conditions, shown as the horizontal trace in Fig. 10 for comparison. The 'failure' of the textured component is not tolerable for the MDT application and, as a result, the minimum friction coefficient of 0.6 includes a safety margin such that slipping of the textured component should never occur. As a result, damage is only a concern if the component in question is required to be taken apart for maintenance and there is a release of hard, loose material into the main engine assembly. The textured shim would normally be replaced at this point anyway. These more practical aspects of the application are yet to be studied in detail.

Fig. 11 shows that increasing the pulse overlap also increases the arithmetic average (S_a) surface roughness of the sample, as was expected, however the roughness does not appear to correspond to the measured friction coefficients. The same trend was observed for several different surface roughness parameters, including RMS roughness (S_q) and peak-to-trough depth (S_t), indicating that, although it will undoubtedly have some effect, the surface roughness is not the most important parameter contributing to the static friction coefficient.

Cross-sections of the laser textured samples are shown in Fig. 12. The surface roughness (S_a) of the original ground surface, shown in Fig. 12a, was measured to be ~0.4 μm. Fig. 12b shows some modulation of the sample surface, however the overall roughness is still comparable to the ground surface. However, Fig. 12c shows a very different structure with the increased roughness and apparent islands of material (which are still connected to the surface out of the plane of the section shown in the image) caused by the ablation and melt ejection processes, respectively. The change in pulse overlap was also found to change the overall visual appearance of the sample dramatically, as shown in Fig. 13.

It is assumed that this colour change is caused by significant oxidation of the steel surface [19,20], with the effect being more pronounced due to the increased energy, and therefore heat, input at higher pulse overlaps. This oxidation, combined with the increased roughness and associated light trapping at high pulse overlaps, can result in extremely dark matt surfaces. It is assumed that the metal oxides formed at the steel surface increase the surface hardness, thus contributing to the friction increase in this region.

3.3.2. *Material comparison*

The dependence of the friction coefficient on the sample material was also investigated, using the nitriding, low alloy and grade 316 steels mentioned in Section 2.2. As before, the pulse

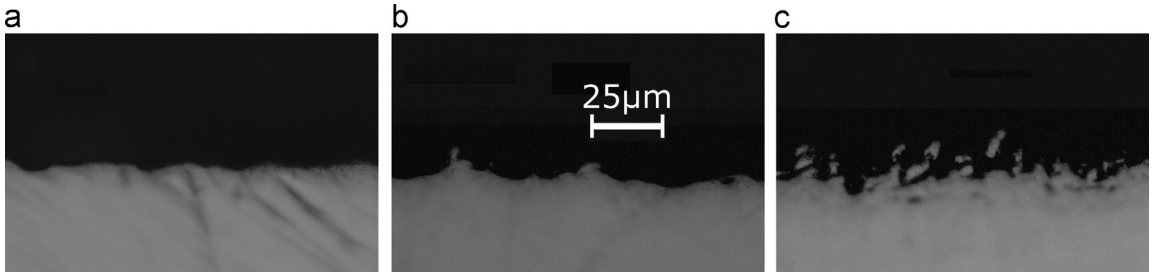

Fig. 12. Cross-sections showing (a) untextured (b) 0% overlap at 0.8 mJ and (c) 75% overlap at 0.8 mJ on SS316.

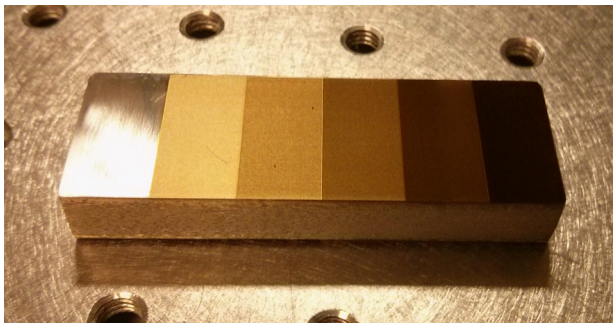

Fig. 13. SS316 sample with different laser processing pulse overlaps for comparison; from left to right: unprocessed, −25%, 0%, 25%, 50% and 75%.

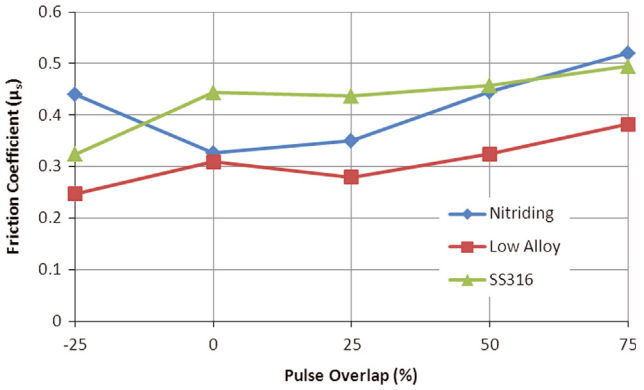

Fig. 14. Friction coefficients as a function of pulse overlap for 3 different materials with the same pulse parameters (25 kHz, 0.8 mJ pulse energy).

overlap of the texturing was varied between −25% and 75%, with the results shown in Fig. 14. The pulse energy used for all samples was 0.8 mJ.

The general trend of increasing friction coefficient with pulse overlap is still visible here, however the maximum friction coefficient achieved is significantly lower than the results reported in Section 3.3.1. This is likely due to the decrease in the normal force applied to the samples (from 60 kN to 40 kN), reducing the true contact area between the two surfaces as the deformation taking place at the surfaces is reduced, however further experiments are required to confirm this. There is also a clear difference in the friction coefficients achieved by the different materials, particularly in the case of the low alloy steel. This is most evident at higher overlaps, where the low alloy steel samples consistently provide ~0.1–0.15 lower friction coefficient compared to the other two sample materials. Unprocessed samples were found to give friction coefficients in the region of 0.2-0.25 for each of the three materials.

Fig. 15 shows the optical micrographs of the three different materials after processing (at 50% pulse overlap); the varying effect of the processing on these materials is visible here, particularly for the SS316, however the *appearance* of the surface is evidently not solely responsible for the achieved friction coefficient.

The processed samples were then tested for hardness, as described in Section 2.3. The results, shown in Fig. 16, show that the laser texturing process increases the surface hardness compared to the as-received sample material. There is also a clear trend of the surface hardness increasing with pulse overlap. The increase in hardness is assumed to facilitate the embedding of the rough sample into the comparatively soft (low alloy) counter-surface when the normal force is applied, increasing the ploughing forces required to move the sample relative to the counter-surfaces. The measurements for both friction and hardness for each sample were therefore plotted against each other, as shown in Fig. 17.

Even with a limited sample size, there appears to be an approximately linear correlation between the surface hardness of the sample and the friction coefficient which can be achieved. It should be noted, however, that whilst most of the measurements point towards this linear relationship, there are some outlying points and so more data should be taken to confirm this trend.

3.4. *Scanning electron microscopy (SEM) analysis*

SEM and EDX measurements were then taken on a variety of differently processed samples in order to confirm which metal oxides are present after laser texturing. Fig. 18 shows several different oxides which are formed on SS316 after laser texturing using a very high pulse overlap (90%). Both thick (up to ~20 μm) and thin (~0.3 μm) oxides generated are chromium rich but also contain nickel and molybdenum. When these measurements were performed on nitriding steel the resulting oxide formation was found to be aluminium and iron rich. These compounds, particularly chromium and aluminium oxides, are very hard materials and so cause the increase in material hardness observed in Section 3.3.2. The low alloy steel does not contain Cr or Al which may explain why this material obtained the lowest friction coefficients (as seen in Fig. 14). The SEM image (top) in Fig. 18 shows a cross-section of the textured surface, with the areas selected for EDX analysis highlighted with four black squares. The thin oxide layers can be seen as thin lines between areas of the base material.

4. Conclusion

The effect of pulse energy and number of pulses on grade 304 stainless steel was examined, with the results providing a basis for a study into the application of nanosecond laser texturing for the generation of high friction surfaces.

In the generation of individual craters, increasing the laser pulse energy increases crater diameter whereas increasing number of pulses increases the crater depth thus allowing independent control over the crater dimensions by optimising laser parameters.

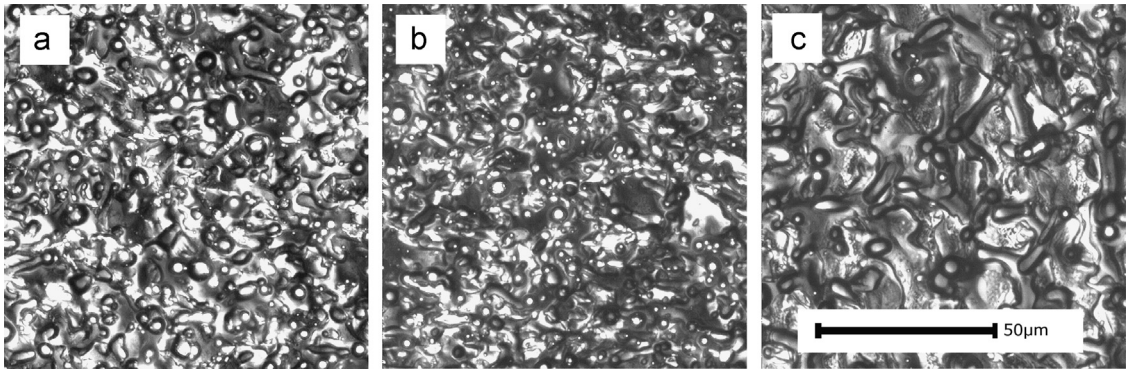

Fig. 15. Micrographs of laser texturing (50% pulse overlap) on three different materials; nitriding steel (a), low alloy steel (b) and SS316 (c).

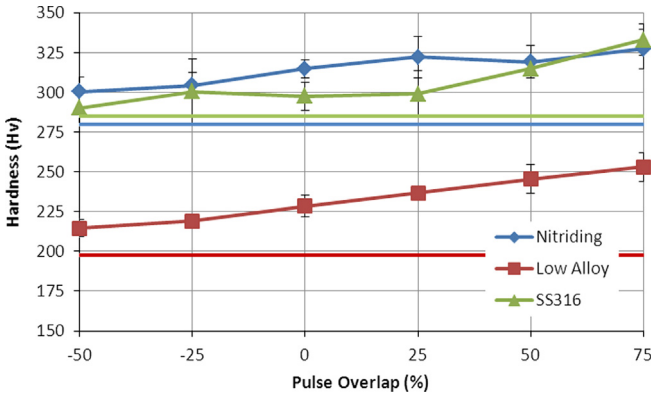

Fig. 16. Surface hardness as a function of pulse overlap for 3 different materials. The straight horizontal lines indicate the hardness of the untextured samples.

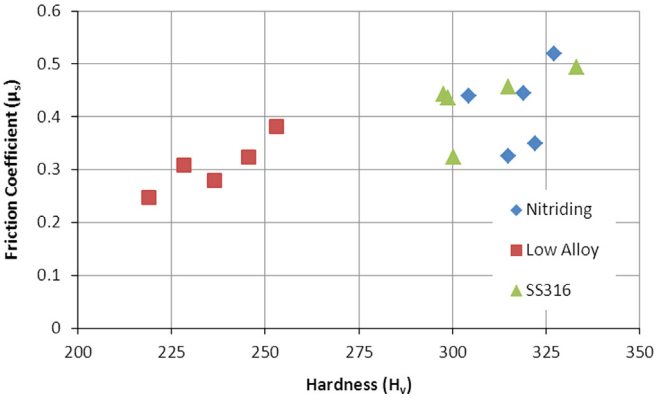

Fig. 17. Relationship between friction coefficient and hardness for 3 different materials and a variety of processing parameters.

This can also be used for overlapping pulses in the generation of lines, where the trough width and depth can be controlled by pulse energy and pulse overlap, respectively. As a general trend, increasing the pulse overlap when processing for high friction applications leads to an increase in surface roughness and the friction coefficient obtained, however no direct correlation between the two was found. Significant oxidation was also observed, particularly at higher pulse overlaps. Increasing the pulse overlap was found to increase the surface hardness of the sample, which appears to have a roughly linear relationship with the obtained friction coefficient. This is most likely due to the formation of a thicker, hard metal oxide layer at the surface which allows deeper embedding of the sample into the counter-surfaces when the normal force is applied.

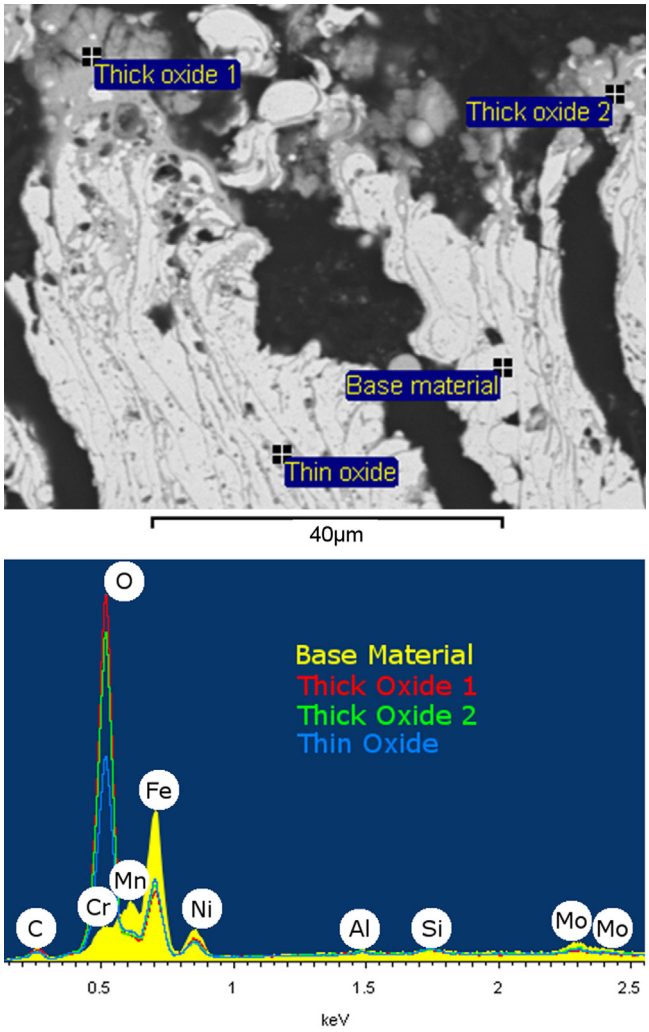

Fig. 18. SEM and EDX analysis of SS316 with very high pulse overlap laser texturing.

Acknowledgements

The authors acknowledge the Engineering and Physical Sciences Research Council (EPSRC) for their support of this research (Grant no. EP/J500227/1).

References

[1] Steen W, Watkins KG, Mazumder J. Laser Material Processing. Springer; 2010.
[2] Etsion I. State of the art in laser surface texturing. J Tribol 2005;127:248.

[3] Nathawat R, Kumar A, Acharya NK, Vijay YK. XPS and AFM surface study of PMMA irradiated by electron beam. Surf Coat Technol 2009;203:2600–4.
[4] Schulze A, Maitz MF, Zimmermann R, Marquardt B, Fischer M, Werner C, et al. Permanent surface modification by electron-beam-induced grafting of hydrophilic polymers to PVDF membranes. RSC Adv 2013;3:22518.
[5] Elsaka SE. Influence of chemical surface treatments on adhesion of fiber posts to composite resin core materials. Dent Mater: Off Publ Acad Dent Mater 2013;29:550–8.
[6] Queiroz JD, Leal AM, Terada M, Agnez-Lima LF, Costa I, Pinto NC, et al. Surface modification by argon plasma treatment improves antioxidant defense ability of CHO-k1 cells on titanium surfaces. Toxicol in vitro: Int J Publ Assoc BIBRA 2013;28:381–7.
[7] Moshkovith A, Perfiliev V, Gindin D, Parkansky N, Boxman R, Rapoport L. Surface texturing using pulsed air arc treatment. Wear 2007;263:1467–9.
[8] Beckford S, Langston N, Zou M, Wei R. Fabrication of durable hydrophobic surfaces through surface texturing. Appl Surf Sci 2011;257:5688–93.
[9] Podgornik B, Vilhena LM, Sedlaček M, Rek Z, Žun I. Effectiveness and design of surface texturing for different lubrication regimes. Meccanica 2012;47:1613–22.
[10] Tang W, Zhou Y, Zhu H, Yang H. The effect of surface texturing on reducing the friction and wear of steel under lubricated sliding contact. Appl Surf Sci 2013;273:199–204.
[11] Kovalchenko A, Ajayi O, Erdemir A, Fenske G. Friction and wear behavior of laser textured surface under lubricated initial point contact. Wear 2011;271:1719–25.
[12] Huang W, Liao S, Wang X. Wettability and friction coefficient of micro-magnet arrayed surface. Appl Surf Sci 2012;258:3062–7.
[13] Wu Z, Deng J, Xing Y, Cheng H, Zhao J. Effect of surface texturing on friction properties of WC/Co cemented carbide. Mater Des 2012;41:142–9.
[14] Duarte M, Lasagni A, Giovanelli R, Narciso J, Louis E, Mücklich F. Increasing lubricant film lifetime by grooving periodical patterns using laser interference metallurgy. Adv Eng Mater 2008;10:554–8.
[15] Vilhena LM, Sedlaček M, Podgornik B, Vižintin J, Babnik A, Možina J. Surface texturing by pulsed Nd:YAG laser. Tribol Int 2009;42:1496–504.
[16] Voevodin AA, Zabinski JS. Laser surface texturing for adaptive solid lubrication. Wear 2006;261:1285–92.
[17] Varenberg M, Halperin G, Etsion I. Different aspects of the role of wear debris in fretting wear. Wear 2002:902–10.
[18] Gabzdyl J, Hansen E. Surface Texturing With ns Pulsed Fiber Lasers. NOLAMP. Trondheim, Norway: Norwegian University of Science and Technology; 2011.
[19] Adams DP, Hodges VC, Hirschfeld DA, Rodriguez MA, McDonald JP, Kotula PG. Nanosecond pulsed laser irradiation of stainless steel 304L: oxide growth and effects on underlying metal. Surf Coat Technol 2013;222:1–8.
[20] Li ZL, Zheng HY, Teh KM, Liu YC, Lim GC, Seng HL, et al. Analysis of oxide formation induced by UV laser coloration of stainless steel. Appl Surf Sci 2009;256:1582–8.